Journal of Power Sources 244 (2013) 115–121

Contents lists available at SciVerse ScienceDirect

Journal of Power Sources

journal homepage: www.elsevier.com/locate/jpowsour

Microstructures and electrochemical performances of nano-sized SiO_x ($1.18 \leq x \leq 1.83$) as an anode material for a lithium(Li)-ion battery

Min Kyung Kim [a], Bo Yun Jang [a,*], Jin Seok Lee [a], Joon Soo Kim [a], Sahn Nahm [b]

[a] Energy Materials and Convergence Center, Korea Institute of Energy Research, Daejeon, Republic of Korea
[b] Department of Materials Science and Engineering, Korea University, Seoul, Republic of Korea

HIGHLIGHTS

- Nano-sized SiO_x was synthesized using an evaporation and condensation process.
- The x-value of the synthesized SiO_x could be controlled by varying the O_2 gas ratios.
- The synthesized SiO_x exhibited a stable cycle performance as an anode.

ARTICLE INFO

Article history:
Received 16 November 2012
Received in revised form
6 March 2013
Accepted 10 March 2013
Available online 22 March 2013

Keywords:
Silicon oxide
Nanoparticle
Nanowire
Microstructure
Electrochemical property
Li-ion battery

ABSTRACT

Nano-sized SiO_x is synthesized by an evaporation and condensation process using induction melting with the injection of various mixed gases. In particular, the effects of O_2 gas on their microstructures and electrochemical properties are investigated. The x-values of the synthesized SiO_x can be controlled from 1.18 to 1.83 by varying the O_2/Ar ratios in the injected gas. A micro-structural analysis reveals that mixture of nanoparticles and nanowires is formed and that the relative amount of nanowire decreases with an increase of the oxygen contents in the injected gas. When x is low, crystalline Si is formed, but this phase disappears when x exceeds 1.28. From the electrochemical analysis of the various SiO_x powders, the Initial Columbic Efficiency (ICE) decreases with the increase in the x-values – largely due to the oxidation of Li-ions such as Li_2O and Li_4SiO_4. Cycle stability, however, is improved with the increase of the x-values, indicating that strain and stress during insertion and extraction of Li-ions are properly released due to the oxide buffer around the Si as well as the nano-sized structure. When $x = 1.18$, a specific capacity of 660 mAh g^{-1} with a columbic efficiency of 99.8% at the 50th cycle is obtained.

1. Introduction

An effective high-capacity secondary battery is required as a key component of electrical vehicles and high-capacity stationary electricity storage systems. Among the various secondary batteries available, Li-ion battery may be a good candidate for such purposes due to its high capacity and well-developed infrastructure. Anode active material has gained a great attention, recently, particularly in connection with the high-capacity Li-ion battery [1–14]. To obtain a high capacity, metal anodes such as Sn and Si have been investigated, instead of graphite, which shows high stability but low capacity. Among metal anodes, Si shows a theoretical capacity as high as 4200 mAh g^{-1} [2–7]. Despite this high capacity, however, a drastic expansion and contraction of volume during the insertion/extraction of the Li-ions limits its application as a new anode material. This huge change in volume leads to pulverization of the anode and a rapid fading of capacity of the battery. As such, various approaches may be adopted to solve the pulverization of the anode [2–14].

One of these approaches entails using nano-sized Si, such as nanoparticles, nanowires or nanotubes [4–7]. Nano-sized Si has a higher tolerance to changes in volume, which improves the cycle performance as a result. Moreover, nano-sized Si has a higher specific area and a shorter diffusion distance of Li-ions, which increases the capacity of the Li-ion. Ning Ding et al. reported that nano-sized Si exhibited a better cyclability than that of micro-sized Si. Specifically, the capacity of nano-sized Si was 738 mAh g^{-1} even after 200 cycles, while that of micro-sized Si dropped to 249 mAh g^{-1}, i.e., only one third that of the nano-sized one [5]. Another approach involves the use of a metal oxide, such as SiO_x, which has attracted special attention recently [5,8–14]. It has been reported that SiO_x ($x \sim 1$) exhibited about 2400 mAh g^{-1} when 1 mol of SiO_x reacted with 4.2 mol of Li-ion during the first lithiation, which was consistent with the discharge [8]. Even though the capacity of SiO_x is lower

* Corresponding author.
E-mail address: byjang@kier.re.kr (B.Y. Jang).

0378-7753/$ – see front matter © 2013 Elsevier B.V. All rights reserved.
http://dx.doi.org/10.1016/j.jpowsour.2013.03.041

than that of Si, it showed good cycling performance due to stress relaxation. Li-oxide (Li_2O) and Li–silicate (Li_4SiO_4), generated by the reaction of Li-ion with SiO_x during the first lithiation, can act as a buffer component [9–12]. M. Miyachi et al. have demonstrated that the presence of a variety of forms (Li_2O, Li_4SiO_4 and Li–Si alloy) serves to enlarge volumetric change and can lead to a good cycling performance of SiO_x with an initial charge capacity of 2404 mAh g^{-1} and a discharge capacity of 598 mAh g^{-1} [13].

According to our previous research, a good cycle performance as well as a high specific capacity can be obtained by using nano-sized SiO_x as an active material for the anode of an Li-ion battery [15]. Nano-sized SiO_x was synthesized by melting Si chunks using an induction heating process and the injection of a mixed gas containing oxygen in order to form SiO_x. Their microstructures and electrochemical properties were investigated. In particular, mixed gases of Ar-balanced O_2 and H_2O were used to oxidize the Si, and the effects of the oxygen ratios in the mixed gas on the properties of the synthesized SiO_x were researched. Unfortunately, it was difficult to control the amount of H_2O vapor using the valve; thus in this study, we focused on the effect of the oxygen ratio on the SiO_x's properties. In addition, a conventional half-cell was fabricated using the synthesized SiO_x as an active material in the anode. The electrochemical properties – such as voltage profiles and cycling performances – were measured to study their dependence on O_2/Ar ratios. The electrochemical properties of the commercial micro-sized SiO_x were measured not only to compare the size effects with those of the synthesized SiO_x but also to evaluate the synthesized SiO_x as an anode material for a high-capacity Li-ion battery.

2. Experimental

Nano-sized SiO_x was synthesized by an evaporation and condensation process by using induction melting and the injection of mixed gases on the Si melt. The details of this process were reported in the previous report [15]. The only difference from our previous researches concerned the use of mixed gases of O_2, H_2O and Ar. The mixture of O_2/Ar gas and H_2O was injected through a copper nozzle on the surface of the melted Si, and the evaporation of the SiO_x was begun. The flow rate of the O_2 varied from 0 to 100 sccm, with that of the Ar gas being 5 slm, which resulted in a volumetric O_2/Ar ratio of 0–2.0%. Simultaneously, 10 ml h^{-1} of the distilled water was injected as a form of vapor through the same nozzle. The water evaporated in the nozzle because of the large difference in pressure and the high temperature of the nozzle. The process parameters and notations for the samples are summarized in Table 1. The evaporated SiO_x vapor was condensed in a process chamber and the solidified powders remained attached to the process chamber wall. Those powders were swept off the wall using a metal mesh and collected in a vial. Microstructure and electrochemical property of a commercial SiO_x (Aldrich, 325-mesh, Lot# MKBG3523V) were also observed to evaluate the nano-sized SiO_x.

The microstructures and crystal structures of the synthesized samples were investigated using a Scanning Electron Microscopy (SEM, Hitachi, S-4700) and X-Ray Diffraction (XRD, Rigaku, HPC-2500) analysis. To determine the valence state of the Si in the SiO_x (which means the x-value in the SiO_x), X-ray Photoelectron Spectroscopy (XPS, Thermo, MultiLab 2000) was used. For the analysis of the XPS spectra, the Si-2p binding energies were: Si (99.8 eV), $SiO_{0.5}$ (100.7 eV), $SiO_{1.0}$ (101.5 eV), $SiO_{1.5}$ (102.5 eV), and $SiO_{2.0}$ (103.5 eV). The value of x was calculated using the following equation:

$$x = (0 \times a) + (0.5 \times b) + (1.0 \times c) + (1.5 \times d) + (2.0 \times e)/(a + b + c + d + e)$$

where, x is the valence state of the Si in the SiO_x, and a, b, c, d and e represent the intensity of Si-2p binding of the Si, $SiO_{0.5}$, $SiO_{1.0}$, $SiO_{1.5}$ and $SiO_{2.0}$, respectively.

The synthesized SiO_x was used as an active material in the Li-ion battery's anode. To form the slurries, 100 mg of SiO_x powders was dispersed in 3.5 ± 0.3 ml distilled water thoroughly using a mortar. The electrode was prepared by coating it with slurries containing active materials (40 wt.%), Denka black (40 wt.%) with Carboxy Methyl Cellulose (CMC), and Styrene Butadiene Rubber (SBR, 20 wt.%, CMC/SBR = 1) as a binder on copper foils. After coating, the electrode was dried for 15 min at room temperature under a vacuum state to prevent pores from appearing on the electrode. Subsequently, the temperature was raised to 90 °C and kept there for 30 min to remove the remaining solvent. The copper foil coated with the electrode material was punched into circular discs with a diameter of 7 mm for use as the working electrode. Coin-type cells (CR2032) were assembled in an Ar-filled glove box using Celgard 2400 as a separator, Li-metal as a count electrode, and 1 M $LiPF_6$ in a mixture of Ethylene Carbonate/DiMethyl Carbonate/Ethyl Methyl Carbonate (EC:DMC:EMC = 1:1:1 in volumetric ratio, Technosemichem, Korea) as an electrolyte. The electrochemical properties were measured by loading the cells on a multi-channel battery system (WBCS 3000, Wanatech Inc.) at 25 °C. The discharge (Li-insertion, lithiation) process was performed galvano-statically at a constant current (CC)/constant voltage (CV) down to a low voltage limit of 0.01 V. The charge (Li-extraction, delithiation) process was carried out at a constant current (CC) up to a high voltage limit of 1.5 V.

Table 1
Summary of process parameters and notations for the samples.

Sample	Ar (slm)	O_2 (Sccm)	H_2O (ml h^{-1})
S1	5	0(0.00%)	10
S2	5	1(0.02%)	10
S3	5	5(0.10%)	10
S4	5	10(0.20%)	10
S5	5	100(2.00%)	10

3. Results and discussion

It is important to determine the valence state of the Si (x-value in SiO_x) of each sample. According to previous researches, x could be obtained from an XPS measurement [16,17]. Fig. 1 shows the Si-2p binding energy spectra of S1, S3, S5 and Ref (the value indicates a valence state of Si). There were five sub-bands according to Si, $SiO_{0.5}$, $SiO_{1.0}$, $SiO_{1.5}$ and $SiO_{2.0}$. In all spectra, the intensity to $SiO_{0.5}$ was negligible, which indicated that $SiO_{0.5}$ was a very unstable phase. S1 consisted of similar amounts of Si, $SiO_{1.0}$ and $SiO_{2.0}$, with the largest amount of $SiO_{1.5}$. Using the equation mentioned above, x was calculated as 1.18. In the case of S3, the amount of Si relatively decreased, which resulted in the increase of x to 1.39. This was obviously caused by further oxidation. On the other hand, S5 showed only a large amount of $SiO_{2.0}$, with relatively small amounts of $SiO_{1.5}$ and $SiO_{1.0}$. S5 was almost in the SiO_2 phase because its valence state was 1.83. Although they are not shown, the spectra of S2 and S4 were similar to those of S1 and S3, respectively. Measurement gave the x-values of S3 and S4 as 1.28 and 1.48, respectively. In summary, there were five samples with x-values of 1.18, 1.28, 1.39, 1.48 and 1.83, respectively. In the case of Ref, x was defined as 1.42, which was similar to S3. However, its spectrum was different from S3's. Ref consisted of a large amount of $SiO_{2.0}$ and a relatively larger amount of Si than S3. This result indicates that Ref consists primarily of Si and $SiO_{2.0}$. Consequently, the SiO_x phase with a valence state of 1.18–1.83 was successively synthesized under the evaporation and condensed process using induction melting with an injection of Ar, O_2 and H_2O gases.

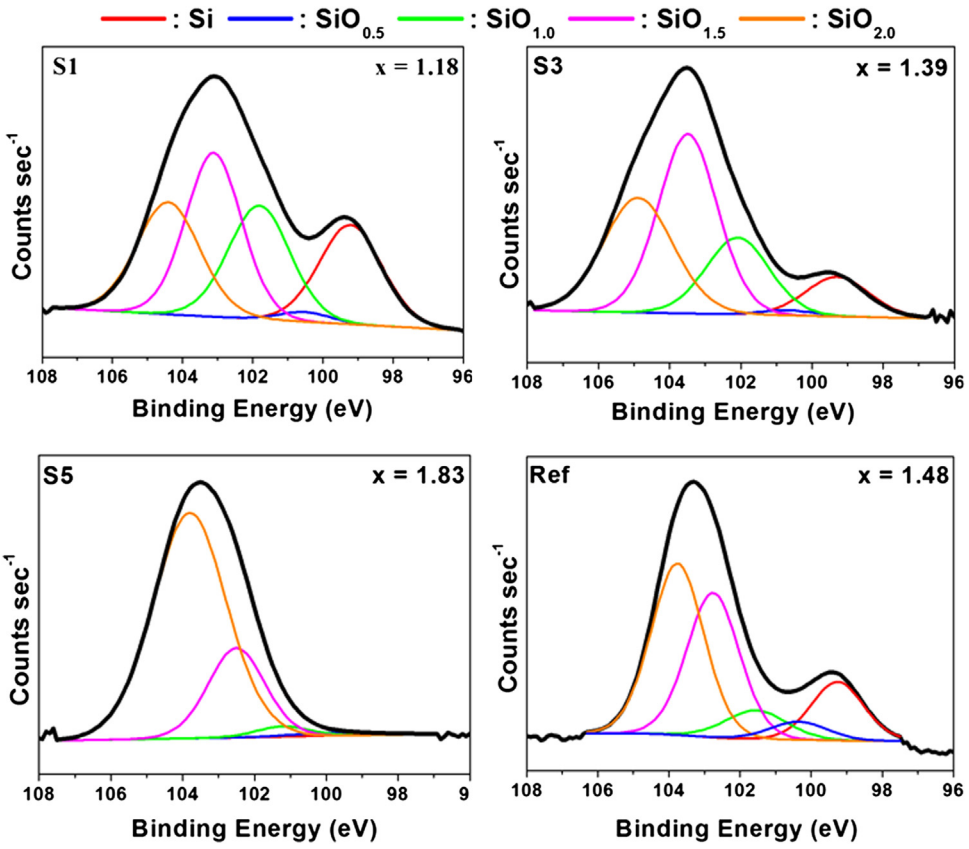

Fig. 1. Si-2p binding energy spectra of S1, S3, S5 and Ref (the value indicates a valence state of Si in SiO_x).

As mentioned in the Experimental procedure, the SiO_x vapor was evaporated and condensed using various gas injections. Those gases determined how much Si was oxidized. The different amount of oxidation resulted in differently colored samples. More specifically, as the amount of O_2 gas increased, further oxidation occurred. Fig. 2 shows the photo images of S1, S2, S3, S4, S5 and Ref powders. As expected, their colors were strongly dependent on their valence states and became brighter when x increased. When $x = 1.18$ (S1), the color was brown (in web version), whereas it was almost white for S5 with $x = 1.83$. It could be understood that further oxidation of Si formed a higher band-gap in the material, which resulted in decreased light absorption in the visible range. Thus, only a white color was observed for S5, which was almost fully oxidized. In the case of Ref, the color was a relatively dark brown, which meant that its x must have been very small. From the XPS measurement, however, x was 1.43, i.e., similar to that of S3. It can be said that the color is also strongly dependent on the particle size. The average particle size of S3 could be measured in nanometers, while that of Ref in micrometers. It may be concluded that the color of the powder offers a simple yet effective clue to determining the synthesized valence state of Si in SiO_x.

Fig. 3 shows SEM images of S1, S2, S3, S4, S5 and Ref. In the case of S1, there were nanowires with a very small amount of nanoparticles. The relative amount of nanoparticles, however, increased with the increase of x. It eventually became difficult to find nanowires in S5. It must be mentioned that the SEM image of any part of each sample showed a similar ratio of nanowires and nanoparticles. From this result, it appears that the injection gas determined not only the valence state but also the nanostructure of the synthesized SiO_x. According to our previous research, only nanoparticles were formed when Ar and oxygen gas were injected [15]. Therefore, H_2O gas might be responsible for the formation of nanowires. However, further investigation of the formation mechanism of nanowires is required. It was also shown that almost all the nanoparticles showed random geometry, indicating that amorphous nanoparticles were mainly formed. According to our previous research, the crystalline silicon nanoparticles were spherical in shape while the amorphous ones displayed random shapes [18]. In addition, the diameters of the nanowires and nanoparticles were independent of the amount of oxidation. The average diameters of the nanoparticles and nanowires were 32–40 nm. On the other hand, micro-sized particles with an average size of 32.5 μm were observed in Ref, as shown in Fig. 3. According to the microstructural analysis, a mixture of nanowires and nanoparticles was formed by the injection of mixed Ar, O_2 and H_2O gas into the Si melt, and the amount of nanoparticles increased in proportion to the O_2/Ar gas ratio.

The crystal structures of the synthesized SiO_x were analyzed by observing the XRD patterns, as shown in Fig. 4. For S1 and S2, there were broad band ranging from 20 to 30° with a small peak at 28.3°. The broad band indicated that this sample consisted mainly of the amorphous phase, namely, SiO_x. The small peak at 28.3° matched that of the Si (JCPDS #75-0589), which meant that there was a crystalline Si phase. As regards S3 and S4, however, only a broad band without any peak was observed, indicating that there was only an amorphous SiO_x phase in these samples. Amorphous SiO_x is better for a Li-ion battery because of its low pulverization of the anode during the charge/discharge process [8]. In addition, the intensities of S3 and S4 were relatively low compared with those of S1 and S2. This is also attributable to the poor crystallinity of S3 and S4. In the case of S5, there was only one band peaking at 21°, which was similar to that of SiO_2. In addition, its intensity was relatively high, which was surely due to the increase of crystallinity. It can be

Fig. 2. Photo images of S1, S2, S3, S4, S5 and Ref.

concluded that amorphous SiO_x with a crystalline Si phase was formed when its valence state was relatively low. However, only an amorphous SiO_x phase was formed when x increased. It should be noted that further research on their structures needs to be conducted to confirm this result because the Si nanowires could influence their structures as well. For Ref, there were three typical bands peaking at 26°, 48°, and 53°, which were from the amorphous SiO_x phase (JCPDS #30-1127).

A low initial irreversible capacity and a long cycle life are two basic requirements for the active material of an anode [19]. Fig. 5 shows the first charge (delithiation)/discharge (lithiation) capacities and ICEs of an anode using S1, S2, S3, S4 and S5 as an active material. The first delithiation capacity of S1 and S2 was 701.17 and 774.64 mAh g^{-1}, respectively. These capacities were much lower than that of Si, which was surely due to the irreversible formation of Li or Li–Si based oxide during the first lithiation. Despite its higher oxygen content, S2 showed a higher capacity than S1, and this result will be discussed later in this paper. The delithiation capacity decreased abruptly for S3 (394.77 mAh g^{-1}) and S4 (346.81 mAh g^{-1}). Although an increase of oxygen content was one reason for this result, the difference between nanowires and nanoparticles could be another reason for this abrupt decrease because the difference in the x-value between S2 and S3 was only 0.1. It might be said that nanowires exhibit better electrochemical properties than nanoparticles. S5 showed very low capacities, obviously because of the high content of SiO_2, as shown in the XPS result. The ICE of the synthesized SiO_x was about 38–43%, which decreased slightly with the increase of x. In addition, compared

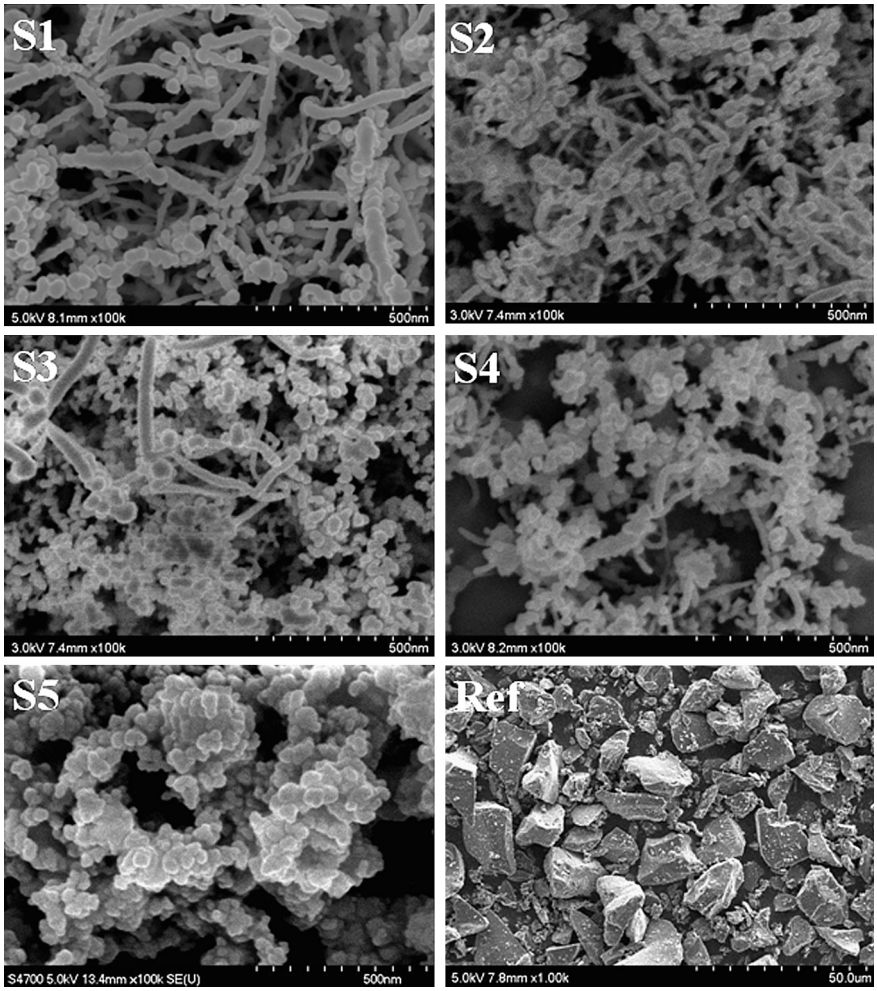

Fig. 3. SEM images of S1, S2, S3, S4, S5 and Ref.

with Ref ($x = 1.43$, first lithiation capacity = 2175 mAh g^{-1}, first delithiation capacity = 1369 mAh g^{-1}, ICE = 63%), S3 shows a much lower capacity and ICE despite its similar x-value. This result could be attributed to the large surface area of the nanostructures, that is to say, a large portion of oxygen can be incorporated into the formation of Li-based oxides such as Li_2O and Li_4SiO_4. Although the data was shown here, the measured specific surface areas of anodes using S1–S5 were higher than 2000 cm^2 g^{-1}. As a consequence, the first charge/discharge capacities as well as the ICE decreased as x increased, and this result was mainly obtained from the formation of Li-based oxides and the increase of the SiO_2 phase which is inactive to the electrical field. In addition, nano structured

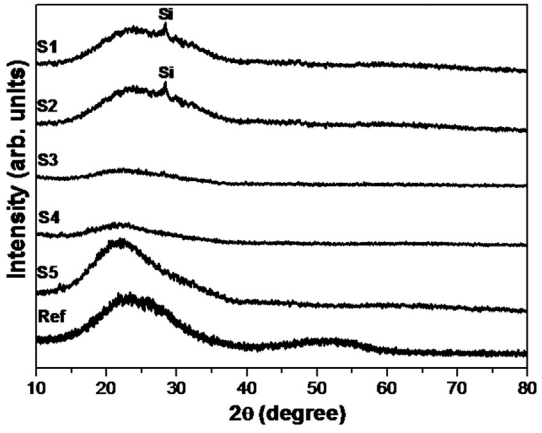

Fig. 4. XRD patterns of S1, S2, S3, S4, S5 and Ref.

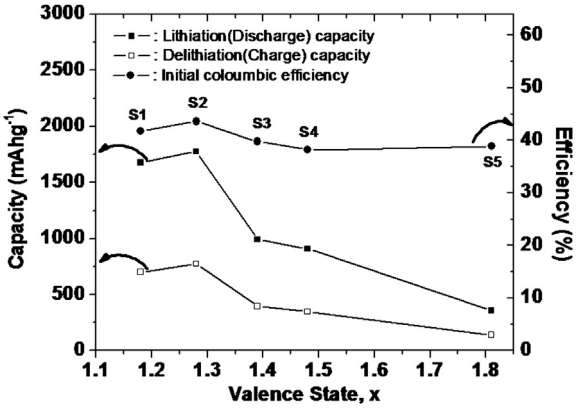

Fig. 5. First charge/discharge capacities and ICEs of an anode using S1, S2, S3, S4 and S5 as an active material.

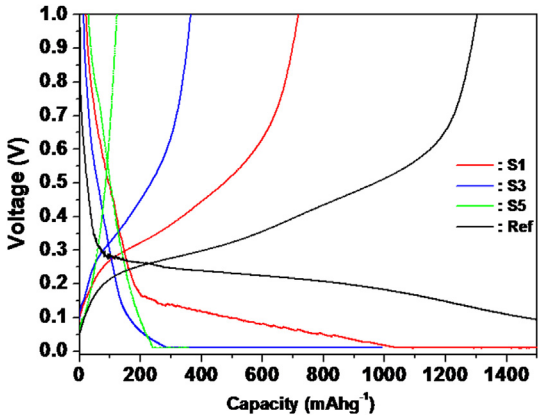

Fig. 6. First charge/discharge voltage profiles of an anode using S1, S3, S5 and Ref as an active material.

SiO_x show relatively low capacities and ICE compared with those of SiO_x micro-particles because of the higher surface area of the nanostructures.

Fig. 6 shows the first charge/discharge voltage profiles of the anode using S1, S3, S5 and Ref as an active material. S2 and S4 exhibited almost similar profiles to those of S1 and S3, respectively. All the corresponding voltages of the synthesized SiO_x were lower than those of SiO_x micro-particles (Ref) during the first lithiation. The voltage profiles showed the same tendency as the first capacities and ICEs. Specifically, S1 corresponded to the lithiation voltage at ca. 0.2 V vs. Li^+/Li, which is obviously due to the alloying of Si and Li. For S3, its corresponding voltage was lower than those of S1. This difference was due to the resistance difference, namely, S3 had a higher resistance to Li-ion because of the higher valence state of Si in SiO_x. It should be mentioned, however, that the nanowires in S1 may be another reason for this result. Excluding S5, no distinguishable plateau from alloying was detected during the insertion/extrusion, thus indicating that only random Li-insertion/extraction occurred [12]. This could be explained by the nano-scaled structure. In other words, there is a large surface area for Li-insertion and a short distance to diffuse in a nano-scaled structure. In the case of S5, a notable plateau at 0.8 V, which was obviously due to the formation of a Secondary Electrolyte Interface (SEI) film on the electrode's surface, was detected [20]. A large amount of SEI was easily formed because there was a large amount of oxygen to incorporate into S5. Consequently, the corresponding voltage for the SiO_x decreased with the increase of the x-value because of the increase of anode resistance. In addition, all the SiO_x showed random Li insertion/extrusion behavior due to the nano-scaled structure, excepting S5, which had a large amount of oxygen to easily form SEI on the anode.

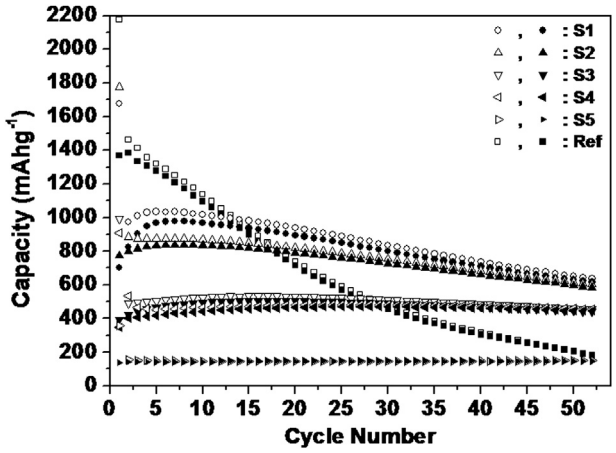

Fig. 7. Cycle performances of the anodes using S1, S2, S3, S4 and S5 and Ref as an active material.

Fig. 7 shows the cycle performances of the anodes using S1, S2, S3, S4 and S5 and Ref as an active material. Although Ref showed the highest first charge/discharge capacity, its capacity faded out quickly with the increase in the number of cycles. On the other hand, the synthesized SiO_x showed a very stable cycle performance. These results were also due to the large portion of Li-based oxides such as Li_2O and Li_4SiO_4 on the nanowires and nanoparticles. Li_2O and Li_4SiO_4 are inactive to an electrical field, but they can serve as a buffer to the expansion of Si during the lithiation process. These buffers can bring about a good cycle performance from the next cycle [9–12]. Moreover, this buffer was more effective in the nano-scale than in the micro-scale. In addition, the anodes using the synthesized SiO_x were not fully charged within several cycles. Especially in the case of S1, the sixth discharge capacity was about 1000 mAh g^{-1} while the first one was only 771 mAh g^{-1}. This result was also due to the microstructural factor of the synthesized SiO_x. There was a huge number of nano-porosities in the fabricated anode, and the electrolyte did not have enough time to fill these nano pores with only one lithiation. Therefore, the Li could not reach inside the electrode to form an alloy with the Si. Looking back at the phenomenon whereby S2 displayed a higher first lithiation/delithiation capacity than that of S1, as shown in Fig. 5, it is now clear that S1 had a lower first lithiation capacity because the Li-ion could not be fully inserted during the first lithiation process. In the cases of S1 and S2, their capacities started to decrease after the full charge. This fading of capacity in S1 and S2 was due to the existence of a crystalline Si phase that was pulverized with the increase in the number of cycles. As a consequence, compared with the SiO_x micro-particles, the cycle performance of the synthesized SiO_x was improved due to the large portion of an effective buffer formed around Si phase. In addition, a full charge could not be obtained within several cycles because there was insufficient time for the electrolyte to reach Si through nano-pore. Despite the fading of capacity, S1, namely, $SiO_{1.18}$ showed 660 mAh g^{-1} at the 50th cycle with a columbic efficiency of 99.8%.

4. Conclusions

Nano-sized SiO_x's with various valence states ($1.18 \leq x \leq 1.83$) were successively synthesized by an evaporation and condensation process using induction melting with the injection of Ar, O_2 and H_2O gas. Their microstructures and electrochemical properties with various O_2 gas ratios were investigated and compared with those of commercial SiO_x microparticles. From the analysis of their microstructures, the synthesized SiO_x consisted of nanowires and nanoparticles. When the x-value increased, the amount of nanoparticles increased, relatively. A crystalline Si phase was observed when x was low whereas only an amorphous SiO_x phase was detected when x was relatively high. Its initial reversible capacity decreased with the increase of the x-value because a larger amount of Li-based oxide was formed during the first lithiation. In addition, the synthesized SiO_x exhibited a relatively lower first discharge capacity but a more stable cycle performance than those of commercial SiO_x. However, SiO_x with a crystalline Si phase showed a fading of capacity which may be due to the pulverization of the crystalline Si phase. $SiO_{1.18}$ showed 660 mAh g^{-1} at the 50th cycle with a columbic efficiency of 99.8%, which means that this sample could be a good candidate for use as an active material in a high capacity Li-ion battery.

Acknowledgments

This research was supported by a grant from the Fundamental R&D Program for Technology of World Premier Materials funded by the Ministry of Knowledge Economy, Republic of Korea.

References

[1] R. Benedek, M.M. Thackeray, J. Power Sources 110 (2002) 406–411.
[2] H. Shin, J. Corno, J. Gole, M. Liua, J. Power Sources 139 (2005) 314–320.
[3] J. Yin, M. Wada, K. Yamamoto, Y. Kitano, S. Tanase, T. Sakai, J. Electrochem. Soc. 153 (3) (2006) A472–A477.
[4] U. Kasavajjula, C. Wang, A. Appleby, J. Power Sources 163 (2007) 1003–1039.
[5] N. Ding, J. Xu, Y. Yao, G. Wegner, I. Lieberwirth, C. Chena, J. Power Sources 192 (2009) 644–651.
[6] H. Ma, F. Cheng, J. Chen, J. Zhao, C. Li, Z. Tao, J. Liang, Adv. Mater. 19 (2007) 4067–4070.
[7] C. Chan, H. Peng, G. Liu, K. McIlwrath, X. Zhang, R. Huggins, Y. Cui, Nat. Nanotechnol. 3 (2008) 31–35.
[8] J. Kim, C. Park, H. Kim, Y. Kim, H. Sohn, J. Electroanal. Chem. 661 (2011) 245–249.
[9] J. Kim, H. Sohn, H. Kim, G. Jeong, W. Choi, J. Power Sources 170 (2007) 456–459.
[10] C. Doh, H. Shin, D. Kim, Y. Ha, B. Jin, H. Kim, S. Moon, A. Veluchamy, Electrochem. Commun. 10 (2008) 233–237.
[11] A. Veluchamy, C. Doh, D. Kim, J. Power Sources 188 (2009) 574–577.
[12] J. Wang, H. Zhao, J. He, C. Wang, J. Wang, J. Power Sources 196 (2011) 4811–4815.
[13] M. Miyachi, H. Yamamoto, H. Kawai, T. Ohta, M. Shirakata, J. Electrochem. Soc. 152 (2005) A2089–A2091.
[14] J. Yang, Y. Takeda, N. Imanishi, C. Capiglia, J.Y. Xie, O. Yamamoto, Solid State Ionics 152–153 (2002) 125–129.
[15] B.Y. Jang, J.S. Lee, J.S. Kim, J. Nanosci. Nanotechnol. 13 (2013) 1–6.
[16] R. Alfonsetti, L. Lozzi, M. Passacantando, P. Picozzi, S. Santucci, Appl. Surf. Sci. 70/71 (1993) 222–225.
[17] F. Teixeira, R. Berjoan, G. Peraudeau, D. Perarnau, Sol. Energy 78 (2005) 763–771.
[18] B.Y. Jang, J.S. Lee, C.H. Ko, J. Korean Phys. Soc. 57 (2010) 1029–1032.
[19] W. Zhang, J. Power Sources 196 (2011) 13–24.
[20] C. Wang, A. Appleby, F. Little, J. Power Sources 93 (2001) 174–185.